JOURNAL OF COMPUTATIONAL PHYSICS **127,** 196–207 (1996)
ARTICLE NO. 0168

Stochastic Simulation of Coupled Reaction–Diffusion Processes

AUDRIUS B. STUNDZIA AND CHARLES J. LUMSDEN

Institute of Medical Sciences and Department of Medicine, University of Toronto, Toronto, Ontario, Canada

Received December 6, 1994; revised February 5, 1996

The stochastic time evolution method has been used previously to study non-linear chemical reaction processes in well-stirred homogeneous systems. We present the first treatment of diffusion, in the stochastic method, for non-linear reaction–diffusion processes. The derivation introduces mesoscopic rates of diffusion that are formally analogous to reaction rates. We map, using Green's function, the bulk diffusion coefficient D in Fick's differential law to the corresponding transition rate probability for diffusion of a particle between finite volume elements. This generalized stochastic algorithm enables us to numerically calculate the time evolution of a spatially inhomogeneous mixture of reaction–diffusion species in a finite volume. The algorithm is equivalent to solving the time evolution of the spatially inhomogeneous master equation. A unique feature of our method is that the time step is stochastic and is generated by a probability distribution determined by the intrinsic reaction kinetics and diffusion dynamics. To demonstrate the method, we consider the biologically important nonlinear reaction–diffusion process of calcium wave propagation within living cells.

1. INTRODUCTION

Spatiotemporal pattern formation is observed in a wide range of physical systems driven far from equilibrium. Processes that exhibit this phenomena include hydrodynamic and thermal convection, parametric wave fronts, solidification fronts, solitons in optics, chemical reaction–diffusion, and biologically excitable media [1]. Mathematical models describing spatiotemporal pattern formation have traditionally been constructed from deterministic equations of motion, usually in the form of nonlinear partial differential equations (NLPDEs). Stochastic noise terms are introduced in either an *ad hoc* manner or derived, with approximations, from the underlying master equation. NLPDEs generally defy analytical solution and much current work has thus focused on the development of techniques for their numerical integration including multigrid, finite element, Monte Carlo, spectral, cellular automata, and lattice boltzmann gas methods [2–4].

One very interesting and elegant approach, based on the idea of stochastic simulation, has been introduced by Gillespie [5–7]. In the Gillespie method a probablistic schedule of simulated encounters between chemical reactants is used to compute the time evolution of reactant concentrations. The stochastic algorithm is rigorous in the sense that it provides an exact solution to the corresponding master equation for chemical reaction in a homogeneous, well-stirred reaction volume [6]. Because the Gillespie method follows unit-by-unit changes in the total numbers of each reactant species, it is especially well suited to the study of systems in which reactant densities are low and the application of methods based on continuum approximations, such as the traditional ordinary differential equations of chemical kinetics, is questionable. This capability is especially relevant to biophysics and cell biology. Within the intact living cell, number densities of key proteins, polynucleotides, and intracellular signaling molecules are typically low [$1–10^2$ μm^{-3}]. Stochastic methods such as that developed by Gillespie are well suited to the computational study of such systems.

However, in contrast to a well-stirred reaction system, the intact living cell is based on a highly complex spatial organization of its constituents, rather than on homogeneous mixing. The reactants mediating, and processed by, the cell's chemical pathways are heterogeneously distributed throughout the cytoplasm and cell membranes. The diffusion of reactant species among localized reaction regions within the cell is therefore a central feature of biophysical chemistry. Although a suitable treatment of diffusion–reaction kinetics for an interacting chemical pathway as has long been available within the continuum approximation suited to high number densities, the lack of a treatment of the spatial diffusion gradient, $D\ \nabla^2\ [C]$, in the stochastic time evolution method has to date prevented its application to spatiotemporal pattern formation. The availability of such a method would open a broad range of intact cellular phenomena to improved computational study.

In this paper, we present an extension of the Gillespie method to reaction–diffusion [RD hereafter] processes in spatially inhomogeneous systems. Our treatment of diffusion enables us to relate, in a well defined manner, the diffusion coefficient D to the corresponding transition rate probability in the multivariate master equation. The method provides a rigorous approach to simulating sto-

0021-9991/96 $18.00

chastic reaction trajectories consistent with this master equation and allows RD kinetics to be treated for low number densities without imposing questionable continuum approximations. To illustrate the new stochastic algorithm and its application in our research, we consider the biologically important nonlinear reaction–diffusion process of calcium (Ca^{++}) wave propagation through the cell interior. Intracellular signaling by means of calcium pulses that propagate from one region of the cell interior to another is a ubiquitous and fundamental means by which intact cells coordinate their spatially distributed patterns of internal structure and function.

2. THE REACTION–DIFFUSION MASTER EQUATION

The principal requirement for a stochastic reaction–diffusion time evolution method is a theory for generating finite time steps, to advance the simulation, determined by the intrinsic reaction kinetics and diffusion dynamics of the system. Consider a volume V that contains $N_{S+} + N_{S-}$ reactant species S_α; $\alpha = 1, ..., N_{S+} + N_{S-}$. The $N_{S+} + N_{S-}$ species can participate in R_μ reversible reactions R_μ; $\mu = 1, ..., N_R$ of the general stochiometric forms

$$m_1 S_1 + m_2 S_2 + \cdots + m_{N_{S+}} S_{N_{S+}} \overset{C_+}{\rightarrow} n_{N_{S+}+1} S_{N_{S+}+1} + n_{N_{S+}+2} S_{N_{S+}+2} + \cdots + n_{N_{S+}+N_{S-}} S_{N_{S+}N_{S-}} \quad (1a)$$

$$n_{N_{S+}+1} S_{N_{S+}+1} + n_{N_{S+}+2} S_{N_{S+}+2} + \cdots + n_{N_{S+}+N_{S-}} S_{N_{S+}+N_{S-}} \overset{C_-}{\rightarrow} m_1 S_1 + m_2 S_2 + \cdots + m_{N_{S+}} S_{N_{S+}}, \quad (1b)$$

where c_+ and c_- are the stochastic rates for a pair of forward and reverse reactions, respectively. A stochastic reaction rate parameter c_μ is defined in the Gillespie procedure such that, to first order in $d\tau$, $c_\mu\, d\tau$ is the average probability that a particular combination R_μ of reactant molecules will collide and react in the reaction volume in the next time interval $d\tau$ [5–7]. If V is the reaction volume, then each c_μ is related to the more familiar deterministic kinetic rate constant k_μ by

$$c_\mu = k_\mu V^d, \quad (2)$$

where d is the power of the spatial dimension in the deterministic kinetic rate constant. We will employ this convention here, but in the context of local volume elements that partition the overall reaction volume V.

We begin our development of the method, by partitioning the reaction-diffusion volume V into a set of finite volume elements (voxels), V_{ijk}; $i = 1, ..., N_x$; $j = 1, ..., N_y$; $k = 1, ..., N_z$, where i, j, and k uniquely label a voxel with lengths L_x, L_y, and L_z along the x, y, and z axes, respectively. To distinguish the real physical surfaces, which bound the total reaction volume V, from the internal boundaries, which are mathematical constructs, we will refer to these internal voxel boundary surfaces as *virtual*. The voxels are chosen to be of sufficiently small size such that the mobile reactants are homogeneously redistributed within each voxel, through collisions with non-reacting species, over the average time step of the simulation. Thus, within each voxel, if the condition that nonreactive collisions occur at a much higher rate than reactive collisions is satisfied, then the stochastic formulation of kinetics is applicable. This condition is generally well satisfied in biophysical systems, where the reactant species are densely surrounded by aqueous solvent.

The bounding surface of V is taken to a be totally reflecting barrier, impermeable to diffusion. Thus the boundary conditions on the concentrations C_α of each of the $\alpha = 1, ..., N_{S+} + N_{S-}$ species are of the Neumann type, with

$$\left.\frac{\partial C_\alpha}{\partial x}\right|_{x=0} = \left.\frac{\partial C_\alpha}{\partial x}\right|_{x=N_x L_x} = 0 \quad (3)$$

and similarly for the y and z axes.

In the treatment of homogeneous reaction systems [5–7], forward and reverse reactions are regarded as two distinct and independent processes. Thus, to develop a unified treatment of reaction–diffusion in this method, we resolve the net diffusive flux of a species S_α across each virtual boundary into two distinct and independent processes: influx and outflux. In contradistinction, solving for Fick's diffusion equation

$$\frac{\partial C_\alpha}{\partial t} = D_\alpha \nabla^2 C_\alpha; \qquad \alpha = 1, ..., N_{S+} + N_{s-} \quad (4)$$

over all the voxels, simultaneously, and taking the spatial gradient yields the average *net* flux at point. On a voxel surface, this net flux is the sum of the fluxes into and out from the voxel treated separately in the stochastic reaction–diffusion method.

To calculate the mean diffusion rate d_α and the corresponding probability density consider the S_α molecules initially within the voxel of interest to be labeled. A labeled molecule can diffuse from the voxel of interest, the ijkth voxel, to an adjacent voxel, one of the $(i \pm 1)jk$th, $i(j \pm 1)k$th, or $ij(k \pm 1)$th voxels. However, once a labeled molecule diffuses out of the voxels adjacent to the voxel of interest to a voxel two voxels away from the voxel of interest, one of the $(i \pm 2)jk$th, $i(j \pm 2)k$th, or $ij(k \pm 2)$th voxels, its label is removed, so that only the remaining, labeled molecules within the voxel of interest contribute

to the subsequent outward diffusion. The unlabelling of a labeled molecule upon crossing a boundary is equivalent to total absorption of the labeled molecule at the boundary. Thus the boundary conditions for the virtual internal boundaries are the Dirichlet type,

$$C_\alpha|_{x=(i+1)L_x} = 0; \quad i = 1, ..., N_x - 2 \tag{5a}$$

$$C_\alpha|_{x=(i-2)L_x} = 0; \quad i = 2, ..., N_x \tag{5b}$$

and similarly for y and z. Applying similar reasoning to voxels that contact the physical boundary of the total reaction volume V we note three possible combinations of boundary conditions along each dimension:

(1) internal voxels with homogeneous

$$C_\alpha|_{x=(i-2)L_x} = C_\alpha|_{x=(i+1)L_x} = 0 \text{ conditions}, \tag{6a}$$

(2) lower bounding voxels with mixed

$$\left.\frac{\partial C_\alpha}{\partial x}\right|_{x=0} = C_\alpha|_{x=2L_x} = 0 \text{ conditions}, \tag{6b}$$

(3) upper bounding voxels with mixed

$$C_\alpha|_{x=(N_x-2)L_x} = \left.\frac{\partial C_\alpha}{\partial x}\right|_{x=N_xL_x} = 0 \text{ conditions}. \tag{6c}$$

Thus there are, in total, nine distinct classes of voxels to consider for the full three-dimensional partitioning.

The mean outward diffusion rates d_α and probability densities are calculated by constructing the Green's function satisfying (4) with finite boundary conditions (5) and (6). Note that this is done only for the S_α concentrations and not for any non-reacting species that constitute the media through which the reacting species diffuse. This procedure is repeated for each of the nine classes of voxels until all the d_α and corresponding probability densities are determined.

The grand probability distribution of the multivariate master equation for the reaction–diffusion system (1) is written as

$$\begin{aligned} P = P(&..., X_{1,ijk}, X_{2,ijk}, ..., X_{N_{S^+},ijk}, \\ &X_{N_{S^+}+1,ijk}, ..., X_{N_{S^+}+N_{S^-},ijk}, ...; t) \end{aligned} \tag{7}$$

wherein the state of the system is defined by the probability of finding $X_{\alpha,ijk}$ molecules of each of the $\alpha = 1, ..., N_{S^+} + N_{S^-}$ species in each one of the $N_xN_yN_z$ voxels. The time evolution of P generated by the chemical kinetics (1) is represented by the reaction part of the RD master equation

$$\begin{aligned} \frac{\partial P}{\partial t} = \sum_{i=1}^{N_x}\sum_{j=1}^{N_y}\sum_{k=1}^{N_z} \{&[c_+h_+\mathbf{E}_{1,ijk}(-m_1)\mathbf{E}_{2,ijk}(-m_2) \\ &\cdots \mathbf{E}_{N_{S^+},ijk}(-m_{S^+})\mathbf{E}_{N_{S^+}+1,ijk}(+n_1) \\ &\times \mathbf{E}_{N_{S^+}+2,ijk}(+n_2)\cdots \mathbf{E}_{N_{S^+}+N_{S^-},ijk}(+n_{N_{S^+}+N_{S^-}})]\, P \\ &+ [c_-h_-\mathbf{E}_{1,ijk}(+m_1)\mathbf{E}_{2,ijk}(+m_2) \\ &\cdots \mathbf{E}_{N_{S^+},ijk}(+m_{N_{S^+}})\mathbf{E}_{N_{S^+}+1,ijk}(-n_{N_{S^+}+1}) \\ &\times \mathbf{E}_{N_{S^+}+2,ijk}(-n_{N_{S^+}+2})\cdots \mathbf{E}_{N_{S^+}+N_{S^-},ijk}(-n_{N_{S^+}+N_{S^-}})]\, P\}, \end{aligned} \tag{8}$$

where we have used the shift operator notation of van Kampen [10], such that

$$\begin{aligned} &\mathbf{E}_{\alpha,ijk}(\pm m_\alpha)P(..., X_{\alpha-1,ijk}, ..., X_{\alpha,ijk}, ..., X_{\alpha+1,ijk}, ...) \\ &\quad = P(..., X_{\alpha-1,ijk}, ..., X_{\alpha,ijk} \pm m_\alpha, ..., X_{\alpha+1,ijk}, ...) \end{aligned} \tag{9a}$$

and

$$\begin{aligned} &\mathbf{E}_{N_{S^+}+\alpha,ijk}(\pm n_{N_{S^+}+\alpha}) \\ &\qquad P(..., X_{N_{S^+}+\alpha-1,ijk}, ..., X_{N_{S^+}+\alpha,ijk}, ..., X_{N_{S^+}+\alpha+1,ijk}, ...) \\ &\quad = P(..., X_{N_{S^+}+\alpha-1,ijk}, ..., X_{N_{S^+}+\alpha,1ijk} \\ &\qquad \pm n_{N_{S^+}+\alpha}, ..., X_{N_{S^+}+\alpha+1,ijk}, ...) \end{aligned} \tag{9b}$$

denote the change in the state of the system, according to the reaction stoichiometry, upon the occurrence of a specific reaction in a particular ijkth voxel. The $h_\pm$ reaction state variables [5, 6] in (8) are given by

$$h_+ = \prod_{\alpha=1}^{N_{S^+}} \frac{X_\alpha!}{m_\alpha!(X_\alpha - m_\alpha)!} \tag{10a}$$

for the forward reaction and

$$h_- = \prod_{\alpha=N_{S^+}}^{N_{S^+}+N_{S^-}} \frac{X_\alpha!}{n_\alpha!(X_\alpha - n_\alpha)!} \tag{10b}$$

for the reverse reaction.

In order to establish transition rates d_α relevant to diffusional transport on the mesoscopic scale of spatial organization represented by a ijkth voxel within V, we will require that the microscopic diffusion dynamics be consistent with the bulk diffusion constant D_α for Fick's differential law

(4). Diffusion between adjacent voxels is then represented in the diffusional part of the RD master equation by

$$\frac{\partial P}{\partial t} = \sum_{i=1}^{N_x}\sum_{j=1}^{N_y}\sum_{k=1}^{N_z}\sum_{\alpha=1}^{N_S} d_\alpha\{X_{\alpha,(i-1)jk}[\mathbf{E}_{\alpha,(i-1)jk}(-1)\mathbf{E}_{\alpha,ijk}(+1)]P + X_{\alpha,(i+1)jk}[\mathbf{E}_{\alpha,ijk}(+1)\mathbf{E}_{\alpha,(i+1)jk}(-1)]P + X_{\alpha,ijk}[\mathbf{E}_{\alpha,(i-1)jk}(+1)\mathbf{E}_{\alpha,ijk}(-1) + E_{\alpha,ijk}(-1)\mathbf{E}_{\alpha,(i+1)jk}(+1)]P\}, \tag{11}$$

where we have again used the shift operator notation

$$\mathbf{E}_{\alpha,(i-1)jk}(\mp 1)\mathbf{E}_{\alpha,ijk}(\pm 1) P(..., X_{\alpha,(i-1)jk}, ..., X_{\alpha,ijk}, ..., X_{\alpha,(i+1)jk}, ...) = P(..., X_{\alpha,(i-1)jk} \mp 1, ..., X_{\alpha,ijk} \pm 1, ..., X_{\alpha,(i+1)jk}, ...) \tag{12}$$

to denote the change in the state of the system as a S_α molecule diffuses from the $(i-1)jk$th voxel to the ijkth voxel or vice versa. As noted above, the mesoscopic d_α transition rate for diffusive particle exchange between voxels is the inverse of the mean time for first escape of a molecule from the ijkth voxel of interest plus the adjacent voxels. It will be calculated below from the first escape probability density constructed using the Green's function solution to the diffusion equation.

3. THE DIFFUSIONAL PROPAGATORS

The Green's function for diffusional particle propagation within V satisfy the same boundary conditions, (5) and (6) , as the concentration. As the boundary conditions for each orthogonal dimension are identical, the formal Green's function solution satisfying the diffusion equation in three dimensions (4) is immediately given by

$$C_\alpha(x,y,z,t) = \int_i^{(i+1)L_x} d\chi \int_j^{(j+1)L_y} d\psi \int_k^{(k+1)L_z} d\zeta \; G_\alpha(x,y,z,t;\chi,\psi,\zeta,t_o=0)C_\alpha(\chi,\psi,\zeta,0); \quad i=0,...,N_x-1; \quad j=0,...,N_y-1; \quad k=0,...,N_z-1. \tag{13}$$

Diffusion is independent in the three orthogonal spatial dimensions. Thus, the Green's function solution in three dimensions is a product of the solutions in each spatial dimension (for identical boundary conditions in each dimension).

Let the time that the a molecule S_α leaves the voxel of interest plus adjacent voxel volumes be τ. Thus,

$$P(\tau \geq t) = P_\alpha(\chi,\psi,\zeta,t). \tag{14}$$

Then the probability $P_\alpha(\chi,\psi,\zeta,t)$ of finding a S_α molecule, within the ijkth voxel plus adjacent voxel volumes, at time t, initially located at (χ,ψ,ζ) within the ijkth voxel, is given by the action of G_α on the initial distribution:

$$P_\alpha(\chi,\psi,\zeta,t) = \int_{(i-2)L_x}^{(i+1)L_x} dx \int_{(j-2)L_y}^{(j+1)L_y} dy \int_{(k-2)L_z}^{(k+1)L_z} dz \; G_\alpha(x,y,z,t;\chi,\psi,\zeta,t_o=0)P_\alpha(\chi,\psi,\zeta,0); \quad i=2,...,N_x-1; \quad j=2,...,N_y-1; \quad k=2,...,N_z-1, \tag{15}$$

where $P_\alpha(\chi,\psi,\zeta,0)$ is normalized to unity. Recall that the voxels are taken to be sufficiently small such that the concentration can be taken to be uniform over a voxel; thus the initial probability density for a particle within any voxel is simply

$$P_\alpha(\chi,\psi,\zeta,0) = P_\alpha(\chi,0)P_\alpha(\psi,0)P_\alpha(\zeta,0) = \frac{1}{L_xL_yL_z}. \tag{16}$$

In order to construct the Green's function solution to the diffusion equation with the finite boundary conditions specified in (5) and (6), consider first the instantaneous source function $G_{\alpha,0}$ solution to the diffusion equation in a region of infinite extent [12]:

$$G_{\alpha,0}(x,y,z,t;\chi,\psi,\zeta,t_o) = \frac{1}{8[\pi D_\alpha(t-t_o)]^{3/2}} \exp\left[-\frac{(x-\chi)^2+(y-\psi)^2+(z-\zeta)^2}{4D_\alpha(t-t_o)}\right]. \tag{17}$$

G_0 represents the probability of finding a particle at position (x,y,z) at time t after instantaneous injection of $X^{(0)}_{\alpha,ijk}$ particles into the ijkth voxel at position (χ,ψ,ζ) at time t_o. In the limit $t \to t_o$, the source function (17) reduces to the delta function:

$$\lim_{t\to t_o} G_{\alpha,0}(x,y,z,t;\chi,\psi,\zeta,t_o) = \delta^{(3)}(x-\chi)(y-\psi)(z-\zeta). \tag{18}$$

Since each voxel is a system with finite boundaries, we apply the method of images; an infinite number of image points or virtual sources, described below, are constructed to satisfy the two boundary conditions per dimension. To illustrate the method we will construct the Green's function satisfying the $G_\alpha|_{\chi=(i-2)L_x} = G_\alpha|_{\chi=(i+1)L_x} = 0$; $i = 2, ..., N_x - 2$ class of boundary conditions (Fig. 1). The others follow similarly.

Consider the three voxel region $[(i-2)L_x, (i+1)L_x]$ with an instantaneous source of $X^{(0)}_{\alpha,ijk}$ particles introduced

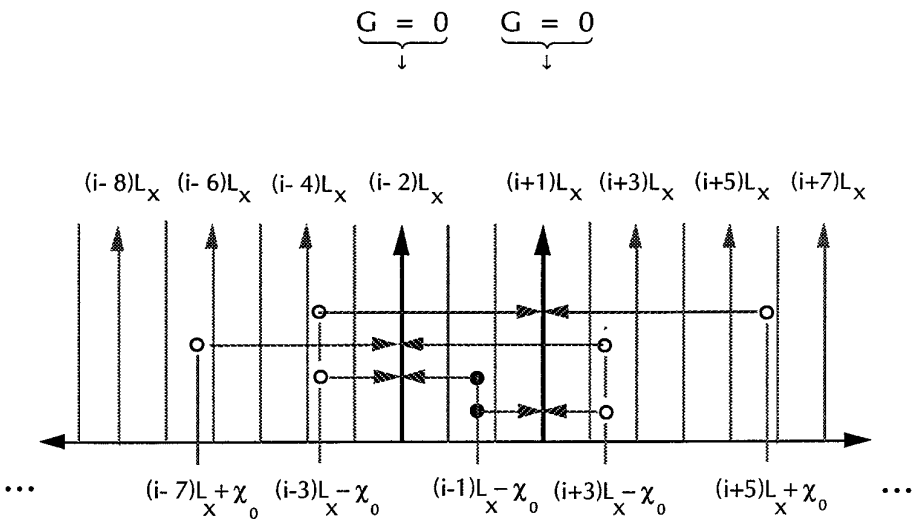

FIG. 1. Method of (infinite) images or virtual sources used to construct the Green's function for diffusion satisfying the absorbing boundary conditions. The absorbing boundaries are indicated by the solid vertical lines at $x = (i - 2)L_x$ and $x = (i + 1)L_x$. The position of the real source is indicated by ● while the positions of the virtual sources are indicated by ○. Antiparallel arrows from the sources indicate concentration ($G = 0$) cancellation at one of the two boundaries.

into the *ijk*th voxel at $(i - 1)L_x + \chi_0$ between $(i - 1)L_x$ and iL_x at time $t = \tau = 0$. After a sufficiently long time, molecules diffuse to $(i - 2)L_x$ and $(i + 1)L_x$ and the flux out of the region of interest is non-zero. But $(i - 2)L_x$ and $(i + 1)L_x$ are the voxel boundaries where we have specified absorbing barriers. Thus, to satisfy the condition that the contribution to the concentration at $(i - 2)L_x$, from the source at $(i - 1)L_x + \chi_0$, vanish we introduce an image point or virtual source at $(i - 3)L_x - \chi_0$. The position and magnitude of the virtual source is chosen such that the net concentration at the boundary is identically zero. The contribution of the virtual source to the distribution of molecules in the finite system is therefore equivalent to the presence of an absorbing boundary at $(i - 2)L_x$.

Similarly, to cancel the flux at $(i + 1)L_x$ from the source at $(i - 1)L_x + \chi_0$, we introduce a virtual source at $(i + 3)L_x - \chi_0$. Half the particles from the real source diffuse, on average, in the $-\chi$ direction and half diffuse, on average, toward $+\chi$. The magnitudes of the virtual sources at $(i - 3)L_x - \chi_0$ and $(i + 3)L_x - \chi_0$ are, therefore, one-half that of the real source at $(i - 1)L_x + \chi_0$. Since the virtual source at $(i - 3)L_x - \chi_0$ also contributes to the flux at both boundaries, to cancel its contribution at $(i + 1)L_x$ we need a new virtual source on the opposite side of this boundary. This new source lies equidistant from the $(i + 1)L_x$ boundary, at $(i + 5)L_x + \chi_0$. Canceling out the contribution of the virtual source at $(i + 3)L_x - \chi_0$ to the concentration at the $(i - 2)L_x$ boundary requires a virtual source at $(i - 7)L_x + \chi_0$. Additional virtual sources are similarly introduced, creating an infinite set of image points on either side of the system boundaries (Fig. 1). Thus, at $x = (i - 2)L_x$, the terms of the infinite series for the absorbing boundary condition are

$$- G_{\alpha,0}\big|_{\substack{x=(i-2)L_x \\ \chi=(i-3)L_x-\chi_0}} + G_{\alpha,0}\big|_{\substack{x=(i-2)L_x \\ \chi=(i-1)L_x+\chi_0}} = 0 \qquad (19a)$$

$$+ G_{\alpha,0}\big|_{\substack{x=(i-2)L_x \\ \chi=(i-7)L_x+\chi_0}} - G_{\alpha,0}\big|_{\substack{x=(i-2)L_x \\ \chi=(i+3)L_x-\chi_0}} = 0 \qquad (19b)$$

$$- G_{\alpha,0}\big|_{\substack{x=(i-2)L_x \\ \chi=(i-9)L_x-\chi_0}} + G_{\alpha,0}\big|_{\substack{x=(i-2)L_x \\ \chi=(i+5)L_x+\chi_0}} = 0 \qquad (19c)$$

and so on, while at $x = (i + 1)L_x$,

$$G_{\alpha,0}\big|_{\substack{x=(i+1)L_x \\ \chi=(i-1)L_x+\chi_0}} - G_{\alpha,0}\big|_{\substack{x=(i+1)L_x \\ \chi=(i+3)L_x-\chi_0}} = 0 \qquad (20a)$$

$$- G_{\alpha,0}\big|_{\substack{x=(i+1)L_x \\ \chi=(i-3)L_x-\chi_0}} + G_{\alpha,0}\big|_{\substack{x=(i+1)L_x \\ \chi=(i+5)L_x+\chi_0}} = 0 \qquad (20b)$$

$$+ G_{\alpha,0}\big|_{\substack{x=(i+1)L_x \\ \chi=(i-7)L_x+\chi_0}} - G_{\alpha,0}\big|_{\substack{x=(i+1)L_x \\ \chi=(i+9)L_x-\chi_0}} = 0 \qquad (20c)$$

and so on. The Green's function satisfying these boundary conditions is

$$G_\alpha(x, t; \chi, t_o) = G_{\alpha,0}[x, t; (i - 1)L_x - \chi; t_0] + \sum_{n=-\infty}^{\infty} \{-G_{\alpha,0}[x, t; (i + 6n + 3)L_x - \chi; t_o] + G_{\alpha,0}[x, t; (i + 6n + 5)L_x + \chi; t_o]\}. \qquad (21)$$

The generalization to three dimensions is immediate. For a voxel with absorbing surfaces on all six boundary faces,

$$G_\alpha(x, y, z, t; \chi, \psi, \zeta, t_o) = G_\alpha(x, t; \chi, t_o) G_\alpha(y, t; \psi, t_o) G_\alpha(z, t; \zeta, t_o). \tag{22}$$

The Green's function satisfying the remaining possible classes of boundary conditions listed can be constructed using analogous arguments.

4. THE DIFFUSIONAL RATES d_α AND THE RD STOCHASTIC SIMULATION ALGORITHM

The non-zero d_α of the diffusional part of the master equation (11) are the mean rates of first passage for a S_α particle within the *ijk*th voxel to any point on the virtual (absorbing) surfaces, furthest from the *ijk*th voxel, of the adjacent voxels. Thus, if $\langle\tau\rangle_\alpha$ is the corresponding mean time to first passage, then

$$d_\alpha = \frac{1}{\langle\tau\rangle_\alpha}, \tag{23}$$

where

$$\langle\tau\rangle_\alpha = \int_0^\infty dt\, t \frac{\partial P_{X_\alpha}(t)}{\partial t} \tag{24}$$

with $P_{X_\alpha}(t)$ the probability density for mean time to first escape, to be constructed next.

The probability density for the mean time to first escape

$$P_{X_\alpha}(\tau > t) = \int_{(i-2)L_x}^{(i+1)L_x} dx \int_{(j-2)L_y}^{(j+1)L_y} dy \int_{(k-2)L_z}^{(k+1)L_z} dz \int_{(i-1)L_x}^{iL_x} d\chi \int_{(j-1)L_y}^{jL_y} d\psi \int_{(k-1)L_z}^{kL_z} d\zeta \times G_\alpha(x, y, z, t; \chi, \psi, \zeta, t_o = 0) P_{X_\alpha}(\chi, \psi, \zeta, 0) \tag{25}$$

of a particle from the *ijk*th voxel, where the fundamental role of the Green's function G_α in the diffusional transition rates is now clear. To summarize, the mean time to first escape is given by

$$\langle\tau\rangle_\alpha = \int_0^\infty dt\, t \frac{\partial P_{X_\alpha}(t)}{\partial t} \tag{26a}$$

$$= \int_0^\infty dt\, P_{X_\alpha}(t) \tag{26b}$$

such that

$$d_\alpha = 1/\langle\tau\rangle_\alpha, \tag{26c}$$

where (26b) is obtained by integrating by parts where for time scales, $D_\alpha(t - t_o)/L^2 > 0.1$, the Green's function solution of $G_\alpha(x, y, z, t; \chi, \psi, \zeta, t_o)$ should be converted [12] into the usual Fourier series solution for large times.

The stochastic hypothesis for reaction processes is

$$c_\mu\, d\tau_R \equiv \text{average probability, to first order in } d\tau_R, \text{ that a particular combination of } R_\mu \text{ reactant molecules will collide and react in the volume } V_{ijk} \text{ of the } ijk\text{th voxel, in the next time interval } d\tau_R. \tag{27a}$$

and for diffusion processes is

$$d_\alpha\, d\tau_D \equiv \text{average probability, to first order in } d\tau_D, \text{ that one of } N_S \text{ molecules will diffuse out of the volume } V_{ijk} \text{ of the } ijk\text{th voxel into an adjacent voxel, in the next time interval } d\tau_D. \tag{27b}$$

Using the stochastic hypothesis (27), we construct the central concept, the reaction–diffusion probability density function, $P(\tau_{\mathrm{RD}}; \mu, \alpha, i, j, k)$, for the stochastic reaction–diffusion method:

$$P(\tau_{\mathrm{RD}}; \mu, \alpha, i, j, k)\, d\tau_{\mathrm{RD}} \equiv \text{the probability at time } t \text{ that either} \tag{28a}$$

(1) the next reaction in the *ijk*th voxel will occur in the differential time interval $(t + \tau_{\mathrm{RD}}, t + \tau_{\mathrm{RD}} + d\tau_{\mathrm{RD}})$, and will be a R_μ reaction of $\mu = 1, ..., N_{\mathrm{R}}$ possible reactions $= P_0(\tau_{\mathrm{RD}}) h_{\mu,ijk} c_\mu\, d\tau_{\mathrm{RD}}$, or (28b)

(2) the next diffusion out of the *ijk*th voxel will occur in the differential time interval $(t + \tau_{\mathrm{RD}}, t + \tau_{\mathrm{RD}} + d\tau_{\mathrm{RD}})$ and will be a D_α diffusion of $\alpha = 1, ..., N_S$ possible diffusive species $= P_0(\tau_{\mathrm{RD}}) X_{\alpha,ijk}\, d_\alpha\, d\tau_{\mathrm{RD}}$, (28c)

where

$$P_0(\tau_{\mathrm{RD}}) \equiv \text{the probability density that no reaction or diffusion occurs in the time interval } (t, t + \tau_{\mathrm{RD}}) \tag{29a}$$

$$= \exp\left\{ -\left[\sum_{i=1}^{N_x} \sum_{j=1}^{N_y} \sum_{k=1}^{N_z} \left[\sum_{\mu=1}^{N_R} h_{\mu,ijk} c_\mu + \sum_{\alpha=1}^{N_S} X_{\alpha,ijk}\, d_\alpha \right) \right] \tau_{\mathrm{RD}} \right\}. \tag{29b}$$

Thus, $P(\tau_{RD}; \mu, \alpha, i, j, k)$ is a joint probability density function on the space of the continuous variable τ_{RD} and the discrete variables μ, α, i, j, k. For reaction-only or diffusion-only systems, (29) reduces to

$$P_0(\tau_R) \equiv \text{the probability density that no reaction occurs in the time interval } (t, t + \tau_R) \quad (30a)$$

$$= \exp\left\{-\left[\sum_{i=1}^{N_x}\sum_{j=1}^{N_y}\sum_{k=1}^{N_z}\left(\sum_{\mu=1}^{N_R} h_\mu c_\mu\right)\right]\tau_R\right\}, \quad \text{or} \quad (30b)$$

$$P_0(\tau_D) \equiv \text{the probability density that no diffusion occurs in the time interval } (t, t + \tau_D) \quad (31a)$$

$$= \exp\left\{-\left[\sum_{i=1}^{N_x}\sum_{j=1}^{N_y}\sum_{k=1}^{N_z}\left[\sum_{\alpha=1}^{N_S} X_{\alpha,ijk}\, d_\alpha\right)\right]\tau_D\right\}, \quad (31b)$$

respectively.

The central result is to numerically simulate, using Monte Carlo techniques (described below), the stochastic reaction–diffusion process generated by $P(\tau_{RD}; \mu, \alpha, i, j, k)$. Note that the finite time step τ_{RD} is not assigned *a priori* to satisfy numerical stability, but it is generated by inversion of the $P_0(\tau_{RD})$ density,

$$\tau_{RD} = -\frac{\ln(r_1)}{\sum_{i=1}^{N_x}\sum_{j=1}^{N_y}\sum_{k=1}^{N_z}\left(\sum_{\mu=1}^{N_R} h_{\mu,ijk}c_\mu + \sum_{\alpha=1}^{N_S} X_{\alpha,ijk}\, d_\alpha\right)}, \quad (31)$$

where r_1 is a random variable uniformly distributed over [0, 1]. Thus, τ_{RD} is not a unique fixed value but a distribution of values characteristic of the intrinsic time scales of the underlying RD processes. A practical consequence of this method for generating τ_{RD} is that numerical stability is guaranteed.

The first reaction or diffusion in the ijkth voxel occurring after τ_{RD} is generated by first calculating the sum of reactions and diffusions over all the voxels

$$a = \sum_{i=1}^{N_x}\sum_{j=1}^{N_y}\sum_{k=1}^{N_z}\left(\sum_{\mu=1}^{N_R} h_{\mu,ijk}c_\mu + \sum_{\alpha=1}^{N_S} X_{\alpha,ijk}\, d_\alpha\right), \quad (32)$$

then finding the partial cumulative sum that is greater than or equal to the quantity $r_2 a$,

$$\sum_{i=1}^{i'-1}\sum_{j=1}^{j'-1}\sum_{k=1}^{k'-1}\left(\sum_{\mu=1}^{\mu'-1} h_{\mu,ijk}c_\mu\right) < r_2 a \le \sum_{i=1}^{i'}\sum_{j=1}^{j'}\sum_{k=1}^{k'}\left(\sum_{\mu=1}^{\mu'} h_{\mu,ijk}c_\mu\right) \quad (33a)$$

$$\sum_{i=1}^{i'-1}\sum_{j=1}^{j'-1}\sum_{k=1}^{k'-1}\left(\sum_{\mu=1}^{N_R} h_{\mu,ijk}c_\mu + \sum_{\alpha=1}^{\alpha'-1} X_{\alpha,ijk}\, d_\alpha\right) < r_2 a \le \sum_{i=1}^{i'}\sum_{j=1}^{j'}\sum_{k=1}^{k'}\left(\sum_{\mu=1}^{N_R} h_{\mu,ijk}c_\mu + \sum_{\alpha=1}^{\alpha'} X_{\alpha,ijk}\, d_\alpha\right), \quad (33b)$$

where r_2 is a second random variable uniformly distributed over [0, 1]. Equations (32a) and (32b) correspond to a reaction and diffusion, respectively.

The RD stochastic simulation algorithm, formatted in a manner that allows it to be compared step by step with the homogeneous system algorithm [5–7], is therefore as follows:

Step 0 (Initialization).

i. Set the time variable $t = 0$.

ii. Specify and store the initial values for the $N_S N_x N_y N_z$ variables $X_{1,ijk}, X_{2,ijk}, \ldots, N_{N_S,ijk}$, where $X_{\alpha,ijk}$ is the initial number of molecules of species S_α in the ijkth voxel V_{ijk}.

For the reaction part of the algorithm:

iii. Specify and store the values of the N_R reaction rates $c_1, c_2, \ldots, c_{N_R}$ for the N_R reactions $\{R_\mu\}$.

iv. Calculate and store the $N_R N_x N_y N_z$ quantities $h_{1,ijk}c_1, h_{2,ijk}c_2, \ldots, h_{N_R,ijk}c_{N_R}$.

For the diffusion part of the algorithm:

v. Specify and store the values of the N_S diffusion rates $d_1, d_2, \ldots, d_{N_S}$ for the N_S reactions $\{D_\alpha\}$.

vi. Calculate and store the $N_S N_x N_y N_z$ quantities $X_{1,ijk}\, d_1, X_{2,ijk}\, d_2, \ldots, X_{N_S,ijk}\, d_{N_S}$.

vii. Specify and store a series of sampling times $t_1 < t_2 < \cdots$ up to a stopping time t_{stop}.

Step 1. Using the Monte Carlo techniques (31) and (32),

i. Generate one set of random variables set $\{\tau_{RD}, \mu, \alpha, i, j, k\}$ according to the joint reaction–diffusion probability density function $P(\tau_{RD}, \mu, \alpha, i, j, k)$.

Step 2. Advance t by the generated time step: τ_{RD}.

For a reaction-driven time step:

i. Update the $X_{\alpha,ijk}$ values of those species involved in reaction R_μ to reflect the occurrence of one R_μ reaction and recalculate the quantities $h_{\nu,i'j'k'}c_\nu$ and $X_{\alpha',i'j'k'}$ for those reactions $\{R_\nu\}$ and diffusions $\{D_{\alpha'}\}$, respectively, whose reactant–diffusant $X_{\alpha',i'j'k'}$ values have just been changed.

For a diffusion-driven time step:

ii. Update the value of the specie involved in diffusion D_α to reflect the occurrence of one D_α diffusion and recalculate the quantities $h_{\nu,i'j'k'}c_\nu$ and $X_{\alpha',i'j'k'}$ for those reac-

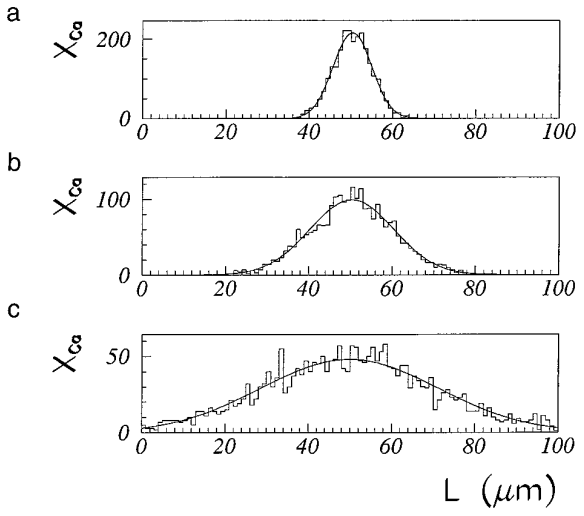

FIG. 2. Stochastic time evolution simulation of diffusion in one dimension. The voxel width is 1 μm. A particle diffusion coefficient of $D_{\text{cyt}} = 10.0\ \mu\text{m}^2\ \text{s}^{-1}$, corresponding to intracellular Ca^{++} diffusion, was used. The initial particle distribution was a 1 μm wide gaussian. This distribution corresponds to an initial delta function distribution situated at 50 μm at time $t = 0$ s. At the sampling times, $t = 1.05$ s , 5.05 s , and 20.05 s, the theoretical gaussian rms widths are 4.58 μm, 10.0 μm, and 20.0 μm, respectively. A gaussian function was fit, using binned maximum likelihood, to the corresponding simulation distributions yielding rms widths of 4.62 ± 0.07 μm, 10.1 ± 0.2 μm, and 21.2 ± 0.4 μm, respectively.

tions $\{R_{\nu'}\}$ and diffusions $\{D_{\alpha'}\}$, respectively, whose reactant-diffusant $X_{\alpha',i'j'k'}$ values have just been changed.

Step 3. i. If t has just been advanced through one of the sampling times t_i, read out the current molecular population values $X_{1,ijk}$, $X_{2,ijk}$, ..., $N_{N_S,ijk}$.

ii. If $t > t_{\text{stop}}$, or if no more reactant–diffusants remain (all $X_{\alpha,ijk} = 0$), terminate the calculation; otherwise return to Step 1 and repeat.

The stochastic RD method, as outlined above, is applicable to models in which the initial conditions are modeled in either a deterministic (delta function distribution of initial conditions) or non-deterministic manner.

The stochastic RD method, as outlined above, is applicable to models in which the initial conditions are modeled in either a deterministic (delta function distribution of initial conditions) or a non-deterministic manner.

In the next section we will present an application of the above stochastic reaction–diffusion algorithm to a simulation of reaction–diffusion Ca^{++} wave propagation in living cells. This process is a remarkable biological example of reaction–diffusion mesoscopic pattern formation in inhomogeneous excitable media. We first show, in Fig. 2, a stochastic time evolution simulation for only the diffusion part of the algorithm. The simulation is in one dimension with a voxel width of 1 μm. A particle diffusion coefficient of $D_{\text{cyt}} = 10\ \mu\text{m}^2\ \text{s}^{-1}$, corresponding order-of-magnitude to *effective* Ca^{++} diffusion in living cells, was used. The initial particle distribution was a 1-μm wide gaussian. This distribution corresponds to an initial delta function distribution situated at 50 μm at time $t = 0$ s. At the sampling times, $t = 1.05$ s , 5.05 s, and 20.05 s, the theoretical gaussian root-mean-square (rms) widths are 4.58 μm, 10.0 μm, and 20.0 μm, respectively. At $t = 0.05$ s the maximum numbers of particles in the distribution corresponds to a concentration of 1 μM. A gaussian function was fit, using binned maximum likelihood, to the corresponding simulation distributions yielding rms widths of 4.62 ± 0.07 μm, 10.1 ± 0.2 μm, and 21.2 ± 0.4 μm, respectively. Thus, our RD algorithm exhibits good numerical accuracy over the time scale of the simulation presented in the next section. Thus, we are able to accurately model the transient phenomena of reaction–diffusion wave propagation in excitable media. Developing new numerical techniques for improving the speed of the stochastic RD algorithm is a current area of active research.

4. APPLICATION TO A SPATIALLY INHOMOGENEOUS RD SYSTEM

Simulation of the dynamics of intracellular signaling processes, such as the calcium signaling pathway, presents a broad range of challenges to computational physics. Signaling processes in cells occur under nonequilibrium thermodynamic conditions, are spatially heterogeneous, are highly coupled, and exhibit highly non-linear response to stimuli. Moreover, a distinguishing feature of intracellular signaling processes is that the number of biologically active molecules per volume element can fall below the small N limit for which the concept of an average concentration is physically meaningful. Thus, the stochastic time evolution method, which utilizes the exact count of the number of particles of each species in a volume element, is a natural method for simulating the dynamics of intracellular signaling.

We will use a model of the propagation of an ionic calcium (Ca^{++}) reaction–diffusion wave through a biological cell to demonstrate our treatment of diffusion in the stochastic time evolution method. Intracellular calcium is a key second messenger within a dynamic signaling pathway that regulates many important cellular processes [13]. Recent experimental work has demonstrated that the intracellular free cytosolic calcium signals can propagate across a cell as concentration waves [14]. Thus, the calcium signal can exhibit a highly inhomogeneous spatio-temporal organization. Models have been developed, using reaction–diffusion NLPDEs, giving good qualitative agreement with data [15–18]. The model cell for our numerical simulation was constructed from 100 sequential cubic voxels of volume 1 μm^3. This length, 100 μm, of our model cell is on the order of the average diameter of sea urchin eggs, a type

of cell used extensively in the field of cell biology to study intracellular calcium-induced calcium-release (CICR) wave propagation.

The reaction–diffusion CICR process can be succinctly described by a non-linear pair of reaction diffusion NLPDEs as

$$\begin{aligned}
&\frac{\partial}{\partial t}[\mathrm{Ca}^{++}]_{\mathrm{cyt}} \\
&\quad = D_{\mathrm{cyt}}\nabla^2[\mathrm{Ca}^{++}]_{\mathrm{cyt}} + \underbrace{k_{\mathrm{IICR}} + k_{\mathrm{PM\ influx}}}_{\text{constant}} \\
&\qquad - k_{\mathrm{IICR\ pump}}[\mathrm{Ca}^{++}]_{\mathrm{cyt}} - k_{\mathrm{PM\ leak}}[\mathrm{Ca}^{++}]_{\mathrm{cyt}} \\
&\qquad + k_{\mathrm{CICR}}\left(\frac{[\mathrm{Ca}^{++}]^4_{\mathrm{cyt}}}{[\mathrm{Ca}^{++}]^4_{\mathrm{cyt}} + K_1^4}\right)\left(\frac{[\mathrm{Ca}^{++}]^2_{\mathrm{CGCS}}}{[\mathrm{Ca}^{++}]^2_{\mathrm{CGCS}} + K_2^2}\right) \\
&\qquad - k_{\mathrm{CICR\ pump}}\left(\frac{[\mathrm{Ca}^{++}]^2_{\mathrm{CGCS}}}{[\mathrm{Ca}^{++}]^2_{\mathrm{CGCS}} + K_3^2}\right) \\
&\qquad + k_{\mathrm{stores\ leak}}([\mathrm{Ca}^{++}]_{\mathrm{IGCS}} + [\mathrm{Ca}^{++}]_{\mathrm{CGCS}}) \qquad (34a)
\end{aligned}$$

$$\begin{aligned}
&\frac{d}{dt}[\mathrm{Ca}^{++}]_{\mathrm{CGCS}} \\
&\quad = k_{\mathrm{CICR\ pump}}\left(\frac{[\mathrm{Ca}^{++}]^2_{\mathrm{CGCS}}}{[\mathrm{Ca}^{++}]^2_{\mathrm{CGCS}} + K_3^2}\right) \\
&\qquad - k_{\mathrm{stores\ leak}}([\mathrm{Ca}^{++}]_{\mathrm{IGCS}} + [\mathrm{Ca}^{++}]_{\mathrm{CGCS}}), \qquad (34b)
\end{aligned}$$

where $[\mathrm{Ca}^{++}]_{\mathrm{cyt}}$ is the free (or cytosolic) intracellular calcium concentration and $[\mathrm{Ca}^{++}]_{\mathrm{IGCS}}$ and $[\mathrm{Ca}^{++}]_{\mathrm{CGCS}}$ are the calcium concentrations in the intracellular IP_3 and calcium gates calcium stores, respectively (see Fig. 3 and Table I). Cooperativity, defined by the Hill coefficient n in

$$\frac{[\mathrm{Ca}^{++}]^n}{[\mathrm{Ca}^{++}]^n + K^n} \qquad (35)$$

corresponds to the number of calcium ions involved in the reaction.

The reaction–diffusion NLPDEs (33) are the first moment equations of the master equation (with truncation of higher moments):

$$\begin{aligned}
\frac{\partial P}{\partial t} = \sum_{i=1}^{100} & d_{\mathrm{cyt}}\{X_{\mathrm{cyt},(i-1)}[\mathbf{E}_{\mathrm{cyt},(i-1)}(-1)\mathbf{E}_{\mathrm{cyt},i}(+1)] \\
&+ X_{\mathrm{cyt},(i+1)}[\mathbf{E}_{\mathrm{cyt},(i+1)}(-1)\mathbf{E}_{\mathrm{cyt},i}(+1)] \\
&- X_{\mathrm{cyt},i}[\mathbf{E}_{\mathrm{cyt},(i-1)}(+1)\mathbf{E}_{\mathrm{cyt},i}(-1)] \\
&- X_{\mathrm{cyt},i}[\mathbf{E}_{\mathrm{cyt},(i+1)}(+1)\mathbf{E}_{\mathrm{cyt},i}(-1)]\}P \\
&+ c_{\mathrm{IICR}}\{h_{\mathrm{IICR},1}[\mathbf{E}_{\mathrm{IGS},1}(-1)\mathbf{E}_{\mathrm{cyt},1}(+1)] \\
&+ h_{\mathrm{IICR},100}[\mathbf{E}_{\mathrm{IGCS},100}(-1)\mathbf{E}_{\mathrm{cyt},100}(+1)]\}P \\
&+ c_{\mathrm{PM\ influx}}[\mathbf{E}_{\mathrm{cyt},1}(+1) + \mathbf{E}_{\mathrm{cyt},100}(+1)]P \\
&+ [(c_{\mathrm{PM\ efflux}}h_{\mathrm{PM\ efflux},1} + c_{\mathrm{PM\ leak}}h_{\mathrm{PM\ leak},1})\mathbf{E}_{\mathrm{cyt},1}(-1)]P \\
&+ [(c_{\mathrm{PM\ efflux}}h_{\mathrm{PM\ efflux},100} + c_{\mathrm{PM\ leak}}h_{\mathrm{PM\ leak},100})\mathbf{E}_{\mathrm{cyt},100}(-1)]P \\
&+ \cdots + c_{\mathrm{IGCS\ pump}}h_{\mathrm{IGCS\ pump},1}[\mathbf{E}_{\mathrm{IGCS},1}(+2)\mathbf{E}_{\mathrm{cyt},1}(-2)]P \\
&+ \sum_{i=1}^{100} c_{\mathrm{CICR}}h_{\mathrm{CICR},i}[\mathbf{E}_{\mathrm{CGCS},i}(-4)\mathbf{E}_{\mathrm{cyt},i}(+4)]P \\
&+ \sum_{i=1}^{100} c_{\mathrm{CGCS\ pump}}h_{\mathrm{CGCS\ pump},i}[\mathbf{E}_{\mathrm{cyt},i}(-2)\mathbf{E}_{\mathrm{CGCS},i}(+2)]P \\
&+ c_{\mathrm{stores\ leak}}\{h_{\mathrm{stores\ leak},1}[\mathbf{E}_{\mathrm{IGCS},1}(-1)\mathbf{E}_{\mathrm{cyt},1}(+1)] \\
&+ \sum_{i=1}^{100} h_{\mathrm{stores\ leak},i}[\mathbf{E}_{\mathrm{CGCS},i}(-1)\mathbf{E}_{\mathrm{cyt},i}(+1)]\}P \qquad (36)
\end{aligned}$$

The effective intracellular diffusion constant for Ca^{++} was taken to be 10 $\mu m^2\ s^{-1}$. Propagation of a $[\mathrm{Ca}^{++}]_{\mathrm{cyt}}$ wave, by reaction–diffusion, across a model cell is shown in Fig. 4a with the corresponding equiconcentration contour plot shown in Fig. 4b. The $[\mathrm{Ca}^{++}]_{\mathrm{cyt}}$ wave exhibits dynamical behaviour characteristic of excitable media including (1) a very rapid onset and rise to maximum concentration height (<0.2 s for our model) once the $[\mathrm{Ca}^{++}]_{\mathrm{cyt}}$ exceeds the calcium gated calcium stores (CGCS release excitation threshold), (2) a slowly decaying excitation plateau (about 4 s duration) followed by a more rapid turnoff (about 2 s duration) and (3) a refractory period (on the order of 8 s) wherein the cell cannot be excited from the quiescent or resting state. In the quiescent state the free cytosolic and CGCS Ca^{++} concentrations are approximately 0.15 μM (90 Ca^{++}ions/1 μm^3 voxel) and 1 μM (600 Ca^{++} ions/1 μm^3 voxel), respectively. At the peak of the excitation $[\mathrm{Ca}^{++}]_{\mathrm{cyt}}$ rises by nearly an order of magnitude to about 1.2 μM. Further analysis of this system will be reported elsewhere.

A snapshot of the average of 10 $[\mathrm{Ca}^{++}]_{\mathrm{cyt}}$ wave runs 10 s after the start of the simulation is shown in Fig. 5. Each data point represents the average $[\mathrm{Ca}^{++}]_{\mathrm{cyt}}$ concentration in each voxel and the errors bars indicate the statistical fluctuation about the mean due to the finite number of Ca^{++} ions.

5. DISCUSSION

We have presented the first treatment of diffusion, in the stochastic time evolution method, for reaction–diffusion processes in which spatial pattern formation may be of paramount importance. The derivation introduces

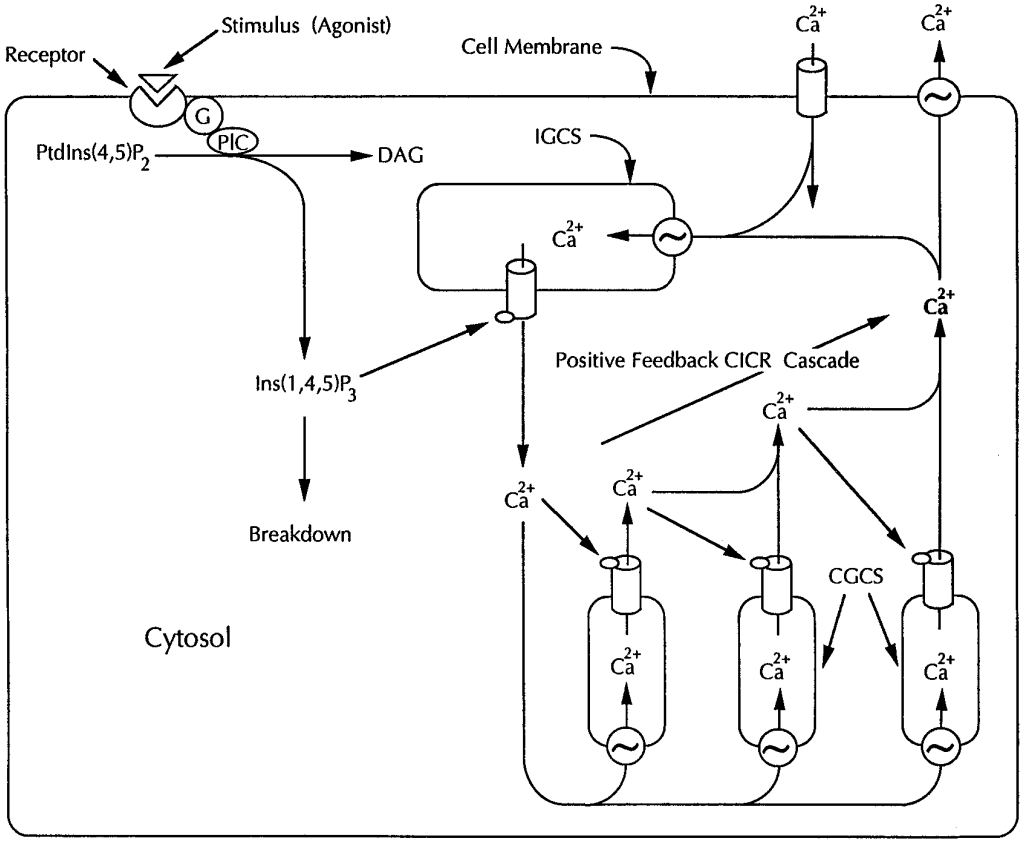

FIG. 3. Two distinct types of Ca^{++} store receptors; an Ins(1, 4, 5)P_3 gated receptor Ca^{++} store (IGCS) and a Ca^{++} gated, but Ins(1, 4, 5)P_3 insensitive, receptor Ca^{++} store (CGCS) are postulated in the calcium-induced calcium-release (CICR) model. The first step leading to $[Ca^{++}]_{cyt}$ wave generation, in this model, is the external stimulus (agonist) induced formation of Ins(1, 4, 5)P_3 via membrane receptor activation: conversion of PtdIns(4, 5)P_3 to Ins(1, 4, 5)P_3. Ins(1, 4, 5)P_3 then gates the IGCS to release primer $[Ca^{++}]_{cyt}$ into the interior (cytosol) of the cell. These pacemaker IGCS were concentrated in the first voxel adjacent to the cell membrane (as suggested by experimental data). The rise in $[Ca^{++}]_{cyt}$ due to release from the IGCS and influx across the cell membrane was taken to occur at a constant rate. Onset of a $[Ca^{++}]_{cyt}$ wave occurs once the local $[Ca^{++}]_{cyt}$ exceeds a threshold level initiating the positive feedback CICR cascade. The wave propagation velocity through the voxels is a function of the interplay of diffusion and the positive feedback of the CICR mechanism. Relaxation to the quiescent state occurs via $[Ca^{++}]_{cyt}$ reuptake by the Ca^{++}-ATPase pump of the IGCS and CGCS and by Ca^{++} extrusion and leakage across the plasma membrane (not shown). In the CICR model, bistability is determined mainly by the competing processes of CICR and calcium reuptake into the CGCS.

TABLE I

Summary of Ca^{++} Reaction Processes in the Model Cell (Fig. 3)

Process	Reaction	Stochastic rate constant
Calcium influx across the cell membrane	$[Ca^{++}]_{ext} \rightarrow [Ca^{++}]_{cyt}$	$c_{PM\ influx} = 37.5\ s^{-1}$
Calcium efflux across the cell membrane	$[Ca^{++}]_{cyt} \rightarrow [Ca^{++}]_{ext}$	$c_{PM\ pump} = 0.35\ s^{-1}$
Ins(1, 4, 5)P_3 induced calcium release (IICR) from the IGCS	$[Ca^{++}]_{IGCS} \rightarrow [Ca^{++}]_{cyt}$	$c_{IICR} = \alpha \cdot 1000 \cdot e^{-2r}\ s^{-1}$
Ins(1, 4, 5)P_3 gated calcium stores (IGCS) pump	$[Ca^{++}]_{cyt} \rightarrow [Ca^{++}]_{IGCS}$	$c_{IGCS\ pump} = 0.18\ s^{-1}$
Calcium induced calcium release (CICR) throughout the cell volume	$2[Ca^{++}]_{cyt} + 4[Ca^{++}]_{CGCS} \rightarrow 6[Ca^{++}]_{cyt}$	$c_{CICR} = 12500\ s^{-1}$
Calcium gated calcium stores (CGCS) pump	$2[Ca^{++}]_{cyt} \rightarrow 2[Ca^{++}]_{CGCS}$	$c_{CGCS\ pump} = 1625\ s^{-1}$
IP_3 and calcium gated calcium stores leak (not shown)	$[Ca^{++}]_{IGCS} \rightarrow [Ca^{++}]_{cyt}$ $[Ca^{++}]_{CGCS} \rightarrow [Ca^{++}]_{cyt}$	$c_{stores\ leak} = 0.1\ s^{-1}$

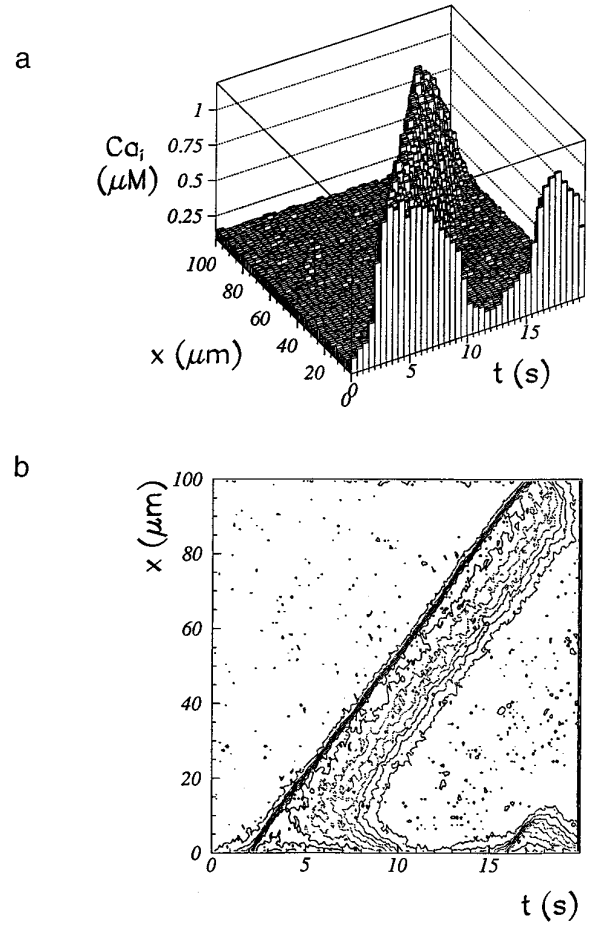

FIG. 4. Propagation of a $[Ca^{++}]_{cyt}$ wave by reaction-diffusion across a model cell is shown in (a) with the corresponding equiconcentration contour plot shown in (b). In the quiescent state, $[Ca^{++}]_{cyt}$ is on the order of 0.15 μM and rapidly rising to about 1.2 μM following excitation. The interwave refractory period is about 8 s in duration.

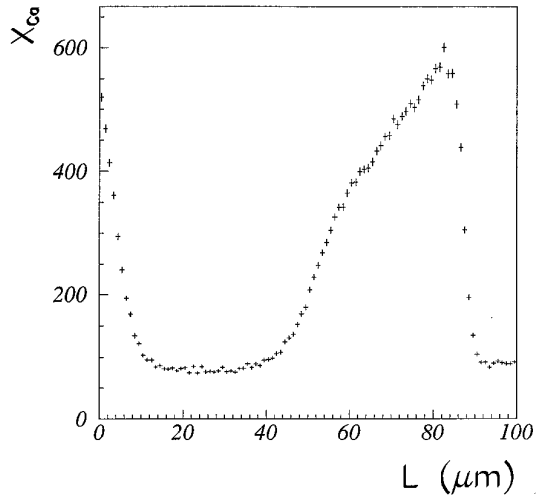

FIG. 5. A snapshot of the average of 10 $[Ca^{++}]_{cyt}$ wave runs 10 s after the start of the simulation. Each data point represents the average $[Ca^{++}]_{cyt}$ concentration in each voxel and the errors bars indicate the statistical fluctuation about the mean due to the finite number of Ca^{++} ions.

mesoscopic rates of diffusion that are formally analogous to reaction rates, and employs these rates to generalize the treatment, heretofore limited to spatially homogeneous systems originally introduced by Gillespie [5–7]. The generalized algorithm enables treatment of reaction–diffusion systems, including the evaluation of regional fluctuations and spatial correlations, in the small particle number limit. It is notable that recent experimental work [19] , wherein individual chemical reactions were observed in solution, has reported an exponential distribution in the interarrival time between successive reaction events, as predicted by the stochastic simulation method [5–7].

The algorithm as presented here is currently limited to reaction–diffusion processes wherein collisions between inert and reacting species occur more frequently than collisions between reacting species. However, this condition is exactly the environment found in biological systems, such as for chemical signaling pathways within individual living cells.

ACKNOWLEDGMENTS

We gratefully acknowledge the support of the Medical Research Council of Canada, operating Grant MA-8635 to C.J.L. and a Postgraduate Training Fellowship to A.B.S from the Department of Medicine, University of Toronto.

REFERENCES

1. M. C. Cross and P. C. Hohenberg, *Rev. Mod. Phys.* **65**, 1 (1993).
2. W. H. Press *et al.*, *Numerical Recipes in C*, 2nd ed. (Cambridge Univ. Press, New York, 1992).
3. M. Markus and B. Hess, *Nature* **347**, 56 (1990).
4. D. Dab, A. Lawniczak, J. P. Boon, and R. P. Kapral, *Phys. Rev. Lett.* **66**, 2462 (1990).
5. D. Gillespie, *J. Comput. Phys.* **22**, 403 (1976).
6. D. Gillespie, *J. Stat. Phys.* **16**, 311 (1976).
7. D. Gillespie, *J. Phys. Chem.* **81**, 2340 (1977).
8. C. J. Lumsden and G. W. Rowe, *J. Phys. Chem.* **81**, 1851 (1984).
9. D. A. McQuarrie, *J. Appl. Probab.* **4**, 413 (1967).
10. N. G. van Kampen, *Stochastic Processes in Physics and Chemistry* (North-Holland, Amsterdam, 1981).
11. M. Kraus, P. Lais, and B. Wolf, *BioSystems* **27**, 145 (1992).
12. A. N. Tikhonov and A. A. Samarskii, *Equations of Mathematical Physics* (Pergamon, Oxford,1963).
13. M. J. Berridge, *Nature* **361**, 315 (1993).

14. J. Lechleiter, S. Gerard, E. Peralta, and D. Clapham, *Science* **252**, 123 (1991); J. Lechleiter and D. Clapham, *Cell* **69**, 283 (1992).
15. K Kuba and S. Takeshita, *J. Theor. Biol.* **93**, 1009 (1981).
16. A. Goldbeter, G. Dupont, and M. Berridge, *Proc. Natl. Acad. Sci. USA* **87**, 1461 (1990).
17. T. Meyer and L. Stryer, *Annu. Rev. Biophys. Biophys. Chem.* **20**, 153 (1991).
18. S. Girard, A. Luckhoff, J. Lechleiter, J. Sneyd, D. Clapham, *Biophys. J.* **61**, 509 (1992).
19. M. Collinson and R. Wightman, *Science* **268**, 1883 (1995).